^{19}F Fast MAS (60-111 kHz) Dipolar and Scalar Based Correlation Spectroscopy of Organic Molecules and Pharmaceutical Formulations

Gal Porat-Dahlerbruch[1], Jochem Struppe[2], Caitlin M. Quinn[1] Angela M. Gronenborn[1,3,4], Tatyana Polenova[1,3,4*]

[1]Department of Chemistry and Biochemistry, University of Delaware, Newark, Delaware 19716, United States; [2]Bruker Biospin Corporation, 15 Fortune Drive, Billerica, MA 01821, United States; [3]Department of Structural Biology, University of Pittsburgh School of Medicine, 3501 Fifth Ave., Pittsburgh, PA 15261, United States; [4]Pittsburgh Center for HIV Protein Interactions, University of Pittsburgh School of Medicine, 1051 Biomedical Science Tower 3, 3501 Fifth Avenue, Pittsburgh, PA 15261, United States

***Corresponding author:** Tatyana Polenova, Department of Chemistry and Biochemistry, University of Delaware, Newark, DE, USA, Tel.: (302) 831-1968; Email: tpolenov@udel.edu

Graphical abstract

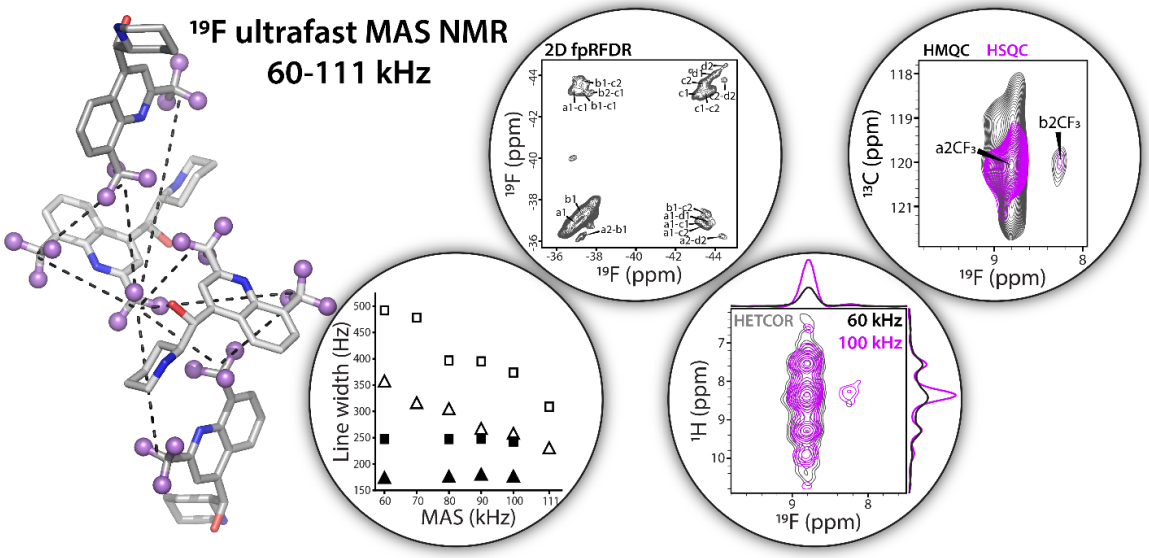

Keywords: high-frequency ^{19}F MAS NMR, ^{1}H decoupling, fluorinated solids, pharmaceutical formulations

Highlights

- High MAS frequencies (60-111 kHz) are advantageous for ^{19}F MAS NMR spectroscopy of organic solids and pharmaceutical formulations.
- ^{1}H decoupling is essential for ^{19}F MAS NMR at MAS frequencies of 60-111 kHz.
- Both dipolar and scalar-based 2D ^{19}F-^{13}C correlation experiments become feasible and efficient at a MAS frequency of 100 kHz.
- High-sensitivity 1D and 2D ^{19}F-detected spectra are acquired with nanomole-quantities of material.

Abstract

^{19}F magic angle spinning (MAS) NMR spectroscopy is a powerful tool for characterization of fluorinated solids. The recent development of ^{19}F MAS NMR probes, operating at spinning frequencies of 60-111 kHz, enabled analysis of systems spanning from organic molecules to pharmaceutical formulations to biological assemblies, with unprecedented resolution. Herein, we systematically evaluate the benefits of high MAS frequencies (60-111 kHz) for 1D and 2D ^{19}F-detected experiments in two pharmaceuticals, the antimalarial drug mefloquine and a formulation of the cholesterol-lowering drug atorvastatin calcium. We demonstrate that ^{1}H decoupling is essential and that scalar-based, heteronuclear single quantum coherence (HSQC) and heteronuclear multiple quantum coherence (HMQC) correlation experiments become feasible and efficient at the MAS frequency of 100 kHz. This study opens doors for the applications of high frequency ^{19}F MAS NMR to a wide range of problems in chemistry and biology.

1. Introduction

^{19}F is a spin-½ nucleus with an intrinsically high gyromagnetic ratio, 100% natural abundance, and a very large chemical shift range, spanning over 300 ppm. These favorable magnetic and physicochemical properties render ^{19}F a powerful NMR probe for structure and dynamics characterization of a wide range of organic and biological molecules [1-3]. Fluorine is absent from virtually all biological systems, yet it can be readily incorporated into proteins and nucleic acids [1, 4-7]. Fluorine atoms are also frequently introduced into pharmaceuticals to enhance metabolic stability and thereby improve therapeutic efficacy [8-10]. In the solid state, ^{19}F NMR spectroscopy has been used to study a variety of fluorinated systems, including organic solids, active pharmaceutical ingredients (APIs) in pharmaceutical formulations, manmade polymers, fluorinated proteins, and protein assemblies [11-24]. ^{19}F NMR observables are sensitive reporters on the structure and dynamics of fluorinated molecules. In solution, ^{19}F paramagnetic relaxation enhancements (PREs) [25], pseudocontact shifts (PCS) [26], and ^{19}F-^{19}F NOEs [27] are commonly used for structural characterization. In solids, the information-rich anisotropic interactions, such as chemical shift and dipolar tensors, are employed [28-30]. Furthermore, owing to the ^{19}F high gyromagnetic ratio, distances as long as ca. 25 and 16 Å are accessible from ^{19}F-^{19}F and ^{19}F-^{13}C based experiments, respectively, making fluorine an attractive nucleus for small-molecule NMR crystallography and protein structure and dynamics characterization [20-23]. In the regime of MAS frequencies above 10-15 kHz, ^{19}F anisotropic interactions are measured through various recoupling techniques [13, 14, 31]. While early ^{19}F MAS NMR experiments were typically performed at spinning frequencies below 20-30 kHz, recent studies have shown that MAS frequencies of 40 kHz and above are beneficial and, in some cases, necessary to achieve the resolution and sensitivity required for the characterization of organic and biological materials [18-20, 32, 33].

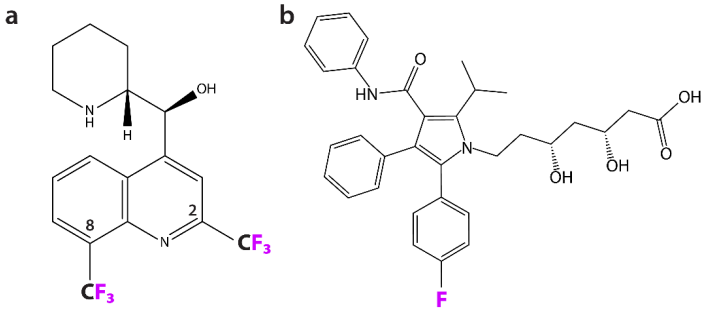

Figure 1. Molecular structure of mefloquine (a) and atorvastatin calcium (b). ^{19}F atoms are colored magenta.

Herein, we systematically evaluate the effect of high MAS frequencies, 60-111 kHz, and ^{1}H decoupling in studies of the antimalarial drug mefloquine hydrochloride and a generic formulation of a cholesterol-lowering drug atorvastatin calcium (Fig. 1) on the resolution of ^{19}F signals. For mefloquine, we show that the long coherence lifetimes of the ^{19}F resonances at the MAS frequency of 100 kHz combined with ^{1}H decoupling greatly improve the performance of 2D dipolar-based, ^{19}F-^{19}F finite-pulse radio frequency-driven recoupling (fpRFDR) [33-36] and ^{1}H-^{19}F heteronuclear correlation (HETCOR) experiments. Remarkably, with 100 kHz MAS, 2D scalar-based correlation experiments become feasible and efficient. To our knowledge, this is the first demonstration of the ^{19}F-^{13}C heteronuclear multiple quantum coherence (HMQC) and heteronuclear single quantum coherence (HSQC) correlation spectra in the solid state.

2. Experimental

2.1. Sample preparation

Mefloquine hydrochloride (100% w/w API) was purchased from Acros Organics. Atorvastatin calcium was a generic formulation manufactured by Teva as 10 mg tablets (6% w/w API) or Apotex as 40 mg tablets (9% w/w API). Herein, we refer these samples as atorvastatin calcium I and II, respectively. All samples were ground and packed into 0.7 mm MAS rotors. Each rotor contained up to 300 µg of mefloquine hydrochloride, atorvastatin calcium I, or atorvastatin calcium II, corresponding to about 600, 27, and 40 nanomoles of API, respectively.

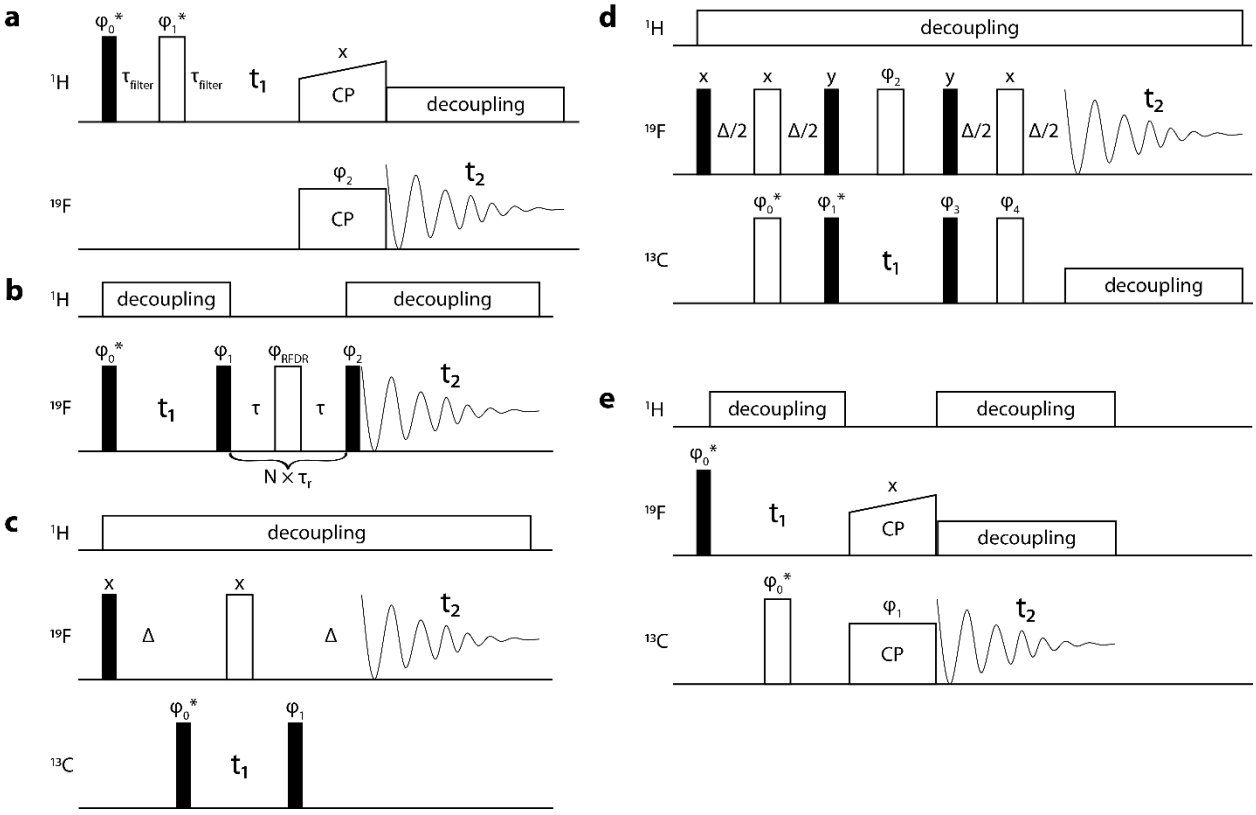

Figure 2. Pulse sequences used herein to record 2D ^{19}F-X correlation experiments: 2D T_2-filtered ^{1}H-^{19}F HETCOR (a), 2D ^{19}F-^{19}F fpRFDR (b), 2D ^{13}C-^{19}F HMQC (c), 2D ^{13}C-^{19}F HSQC (d), and 2D ^{19}F-^{13}C HETCOR (e). 2D T_2-filtered ^{1}H-^{19}F HETCOR phase cycle: φ_0=y-y, φ_1=y, φ_2=xx-x-x yy-y-y, φ_{rec}=x-x-xx y-y-yy. 2D ^{19}F-^{19}F fpRFDR phase cycle: φ_0=x, φ_1=x-x, φ_2=xx -x-x, φ_{rec}=x-x -xx, φ_{RFDR} follows the XY8$_4$[1] scheme [37]. 2D ^{13}C-^{19}F HMQC phase cycle: φ_0=x-x, φ_1=xx -x-x, φ_{rec}=x-x -xx. 2D ^{13}C-^{19}F HSQC phase cycle: φ_0=x*8 -x*8, φ_1=x-x, φ_2=xx -x-x, φ_3=xxxx -x-x-x-x, φ_4= x*8 -x*8, φ_{rec}=x-xx-x -xx-xx. 2D ^{19}F-^{13}C phase cycle: φ_0=y-y, φ_1=xx-x-x yy-y-y, φ_{rec}=x-x-xx y-y-yy. Phases marked with an asterisk are incremented according to the States-TPPI scheme for phase-sensitive indirect detection [38]. The delays in the figure are τ_{filter} = 400 µs, τ = (1/3)*ν_r, where ν_r is the MAS frequency, and Δ = 1/2J = 2 ms for J = $^{1}J_{FC}$ ~250 Hz.

2.2. MAS NMR spectroscopy

All experiments were performed on an 11.7 T Bruker Avance Neo NMR spectrometer equipped with a 0.7 mm HFXY probe (mefloquine and atorvastatin calcium I) and a 0.7 mm H/FX probe (atorvastatin calcium I and II). ^{1}H, ^{19}F, and ^{13}C Larmor frequencies were 499.81 MHz, 470.29 MHz, and 125.68 MHz, respectively. 1D spectra were recorded with ^{1}H-^{19}F cross-polarization (CP) (atorvastatin calcium I) and ^{19}F direct-polarization (DP) excitation (mefloquine

and atorvastatin calcium I and II) at MAS frequencies ranging from 60 to 111 kHz, with and without low-power time-proportional-phase-modulation (TPPM) ^{1}H decoupling [39-41], 'slTPPM' sequence. 2D ^{19}F-^{19}F/^{1}H/^{13}C correlation spectra of mefloquine were recorded at the MAS frequency of 60 and/or 100 kHz. 2D ^{19}F-^{19}F correlation spectrum of atorvastatin calcium II was recorded at the MAS frequency of 111 kHz. The 2D experiments pulse sequences are shown in Fig. 2, and the experimental and processing parameters are detailed in Supporting Information Tables S1 and S2. All datasets were processed and analyzed with Bruker TopSpin 4.1.3. For mefloquine 1D ^{19}F NMR spectra, the overlapping ^{19}F peaks were fitted using the 'solid lineshape analysis' (SOLA) package for accurate line width analysis. The signal-to-noise ratios (SNRs) were calculated on spectra processed without apodization and correspond to the most intense peak.

2.3. Calculation of Bloch-Siegert shifts

The Bloch-Siegert shift Δ_{BS}, in units of ppm, for heteronuclear decoupling is governed by the equation:

$$\Delta_{BS} = \frac{(\gamma_{obs} B_1)^2}{\nu_0^2 - \nu_{irr}^2} \cdot 10^6 = \frac{\left(\gamma_{obs}/\gamma_{irr}\right)^2 \cdot 10^6}{\nu_0^2 - \nu_{irr}^2} \nu_1^2$$

with ν_0 the Larmor frequency of the observed nucleus in units of Hz, ν_1 the radiofrequency (RF) field magnitude (B_1) in units of Hz, ν_{irr} the frequency of applied field in Hz, and γ_{obs} and γ_{irr} are the gyromagnetic ratios of the observed and irradiated nuclei, respectively, in units of Hz/T [42, 43]. Generally, Bloch-Siegert shifts follow a quadratic relation between the RF field, ν_1, and the difference in Larmor frequencies, $\Delta\nu$.

To fit the experimental data, a general quadratic equation of the form $y = ax^2 + b$ was used, where:

$$a = \frac{\left(\gamma_{obs}/\gamma_{irr}\right)^2}{\nu_0^2 - \nu_{irr}^2} \cdot 10^6$$

The theoretical value of parameter a is -3.09·10^{-11} ppm/Hz^2, calculated using the experimental ^{1}H and ^{19}F Larmor frequencies, see above, and known gyromagnetic ratios. Experimental data were fitted to the same equation using MATLAB [44] and the experimental value of a was extracted.

3. Results and Discussion

^{19}F 1D spectra of mefloquine and atorvastatin calcium I at a MAS frequency of 100 kHz are shown in Fig. 3a,b. In mefloquine, the 2CF_3 and 8CF_3 groups give rise to several distinct sets of signals each, corresponding to crystallographically inequivalent sets of fluorine atoms. Resolving individual resonances for the three crystallographically inequivalent molecules in the unit cell in 1D ^{19}F spectra is not possible, even with MAS frequencies as high as 40-60 kHz, ^{1}H decoupling, or selective excitation pulses, necessitating 2D experiments [20]. This is the case even at the MAS frequency of 100 kHz with ^{1}H decoupling, as shown in Fig. 3a. We note that, while we chose to use TPPM ^{1}H decoupling, no comprehensive study of ^{1}H decoupling schemes in ^{19}F-edited fast MAS NMR experiments has been reported to date.

The two ^{19}F resonances in the atorvastatin calcium I spectrum also correspond to the crystallographically inequivalent fluorine atoms in the crystal structure and were assigned by us in an earlier study [19], see Fig. 3b.

The MAS frequency dependences of the line widths for 60-100 kHz spinning, with and without ^{1}H decoupling, are shown in Fig. 3c,d. For mefloquine, ^{19}F lines are getting progressively narrower with increasing MAS frequency, from 154 Hz ($2CF_3$) and 256 Hz ($8CF_3$) at 60 kHz to 120 Hz ($2CF_3$) and 180 Hz ($8CF_3$) at 100 kHz. ^{1}H decoupling reduces the line widths further, to 92 Hz ($2CF_3$) and 167 Hz ($8CF_3$) at 100 kHz, see Fig. 3c. Interestingly, the combination of decoupling and higher MAS frequencies influences the $2CF_3$ and $8CF_3$ resonances differently. The widths of the $2CF_3$ and $8CF_3$ peaks with ^{1}H decoupling at the MAS frequency of 60 kHz are 105 and 212 Hz, but at the MAS frequency of 100 kHz without ^{1}H decoupling the widths are 120 and 180 Hz. As discussed above, each of the two peaks comprises multiple species corresponding to crystallographically inequivalent molecules in the unit cell and the isotropic chemical shifts of the individual species as well as ^{19}F-^{19}F and ^{19}F-^{1}H dipolar couplings contribute to the peak widths. The dipolar coupling contribution to the line widths is reduced with increased MAS frequency and decoupling. These results, together with our previous work on mefloquine and the ^{19}F-^{19}F distances in the mefloquine crystal structure [20], indicate that homonuclear dipolar couplings are a significant source of line broadening in mefloquine ^{19}F spectra. The narrowest lines are achieved at the MAS frequency of 100 kHz when ^{1}H decoupling is applied.

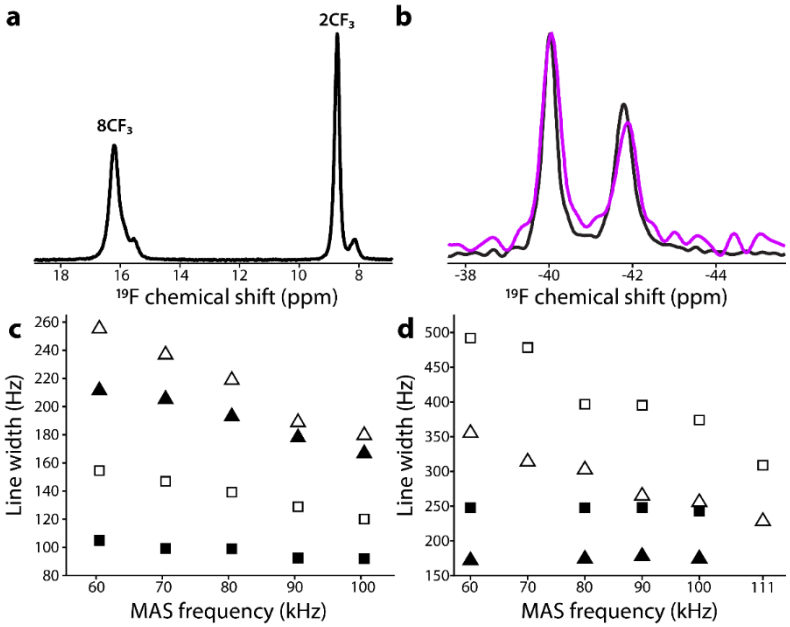

Figure 3. a) ^{1}H-decoupled ^{19}F DP spectrum of mefloquine at the MAS frequency of 100 kHz. The spectrum was acquired with 4 scans; the SNR was 390. **b)** ^{19}F CP and DP spectra of atorvastatin calcium I acquired at the MAS frequency of 100 kHz with ^{1}H decoupling (black) and 111 kHz without ^{1}H decoupling (magenta), respectively. The spectra were acquired with 1,024 and 80 scans; the SNR were 65 and 20, respectively. **c)** Effect of MAS frequencies and ^{1}H decoupling on ^{19}F line widths of mefloquine DP experiments. **d)** Effect of MAS frequencies and ^{1}H decoupling on ^{19}F line widths of atorvastatin calcium I in DP and CP experiments at the MAS frequencies 60-100 and 111 kHz, respectively. Low-power TPPM ^{1}H decoupling RF fields were set to 1/8 and 1/4 of the MAS frequency for mefloquine and atorvastatin calcium I, respectively. Empty and filled symbols indicate line widths measured without and with ^{1}H decoupling, respectively. Mefloquine ^{19}F

peaks with chemical shifts of 16.2 ppm ($8CF_3$) and 8.8 ppm ($2CF_3$) are shown as triangles and squares, respectively. Atorvastatin calcium I ^{19}F peaks with chemical shifts of -40.1 and -41.9 ppm are shown as triangles and squares, respectively. Mefloquine ^{19}F peak assignments were reported in [20].

Interestingly, the influence of spinning frequencies and decoupling on ^{19}F line widths of atorvastatin calcium I is markedly different from that for mefloquine, see Fig. 3d. In atorvastatin calcium I, ^{1}H decoupling at the MAS frequency of 60 kHz results in lines narrowing from 492/357 to 248/173 Hz, while in mefloquine, the line narrowing due to ^{1}H decoupling was more modest, with line widths changing from 256/154 Hz to 212/105 Hz. A significant narrowing of atorvastatin calcium I ^{19}F peaks is observed when applying ^{1}H decoupling at all MAS frequencies tested here, 60-111 kHz. Interestingly, with ^{1}H decoupling, spinning faster than 60 kHz does not narrow the ^{19}F lines further. This implies that ^{1}H-^{19}F dipolar couplings contribute predominantly to the ^{19}F line widths of atorvastatin calcium I at the MAS frequencies up to 111 kHz, confirming our previous report that in dilute systems ^{19}F-^{19}F dipolar couplings are practically negligible.

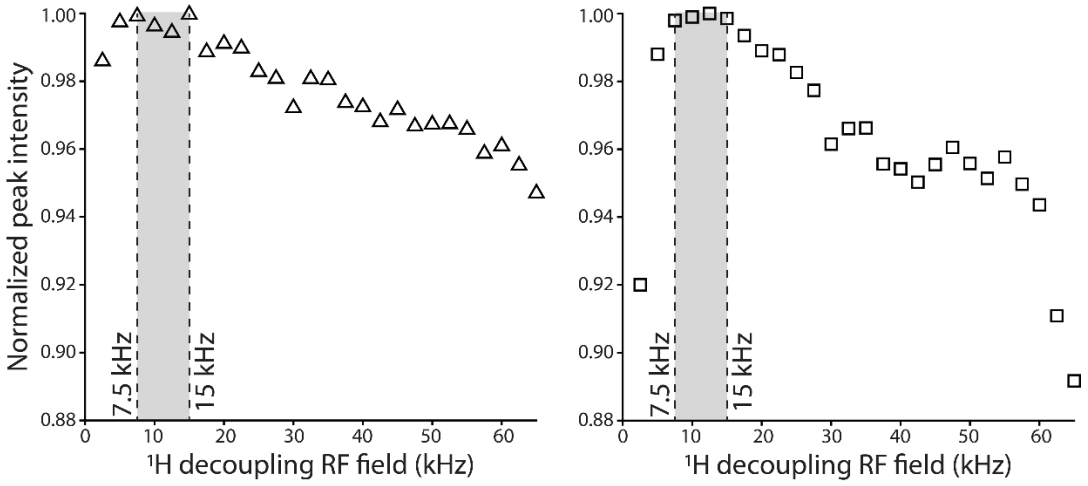

Figure 4. Dependence of ^{19}F peak intensities of mefloquine ^{19}F resonances on the ^{1}H decoupling RF field at 100 kHz MAS frequency. Peak intensities for mefloquine ^{19}F peaks at 16.2 ($8CF_3$) and 8.8 ($2CF_3$) ppm are shown by triangles and squares, respectively. The optimal ^{1}H decoupling RF field strength is indicated by the grey areas.

The efficiency of low-power ^{1}H TPPM decoupling [39-41] for ^{19}F DP experiments of mefloquine at 100 kHz MAS is shown in Fig. 4. Optimal ^{1}H decoupling is achieved at weak RF fields of 7.5 to 15 kHz, or about 1/8 the MAS frequency. Notably, small, but pronounced systematic shifts in the position of the ^{19}F isotropic peaks as a function of the applied ^{1}H decoupling RF field are observed (Fig. 5a). The frequency dependence of both CF_3 peaks follow a quadratic function, suggesting as its cause a Bloch-Siegert shift [45-47]. The experimental values of *a* in a fit of the form $y=ax^2+b$ were $-2.75\cdot10^{-11}$ and $-2.66\cdot10^{-11}$ ppm/Hz^2 for mefloquine $2CF_3$ and $8CF_3$ resonances, respectively, very close to the calculated theoretical value of $-3.09\cdot10^{-11}$ ppm/Hz^2 (see the experimental section). We ruled out that the observed shifts originate from sample heating upon RF irradiation since the shift for increasing temperatures is in opposite direction to the shift induced by the RF irradiation (Fig. 5b). One possible explanation to the lower observed value of *a* is the use of a phase-modulated decoupling scheme, feasibly introducing a delay on

the order of tens of nanoseconds between the decoupling pulses and thus resulting in a lower effective RF field during the acquisition period. Given that the optimal RF fields for ^{1}H decoupling are 7.5-15 kHz (see Fig. 5a grey area), any Bloch-Siegert shifts are expected to be small compared to the ^{19}F line width (<0.01 ppm Bloch-Siegert shift versus >0.2 ppm line width, hence <5% error), and therefore should be negligible.

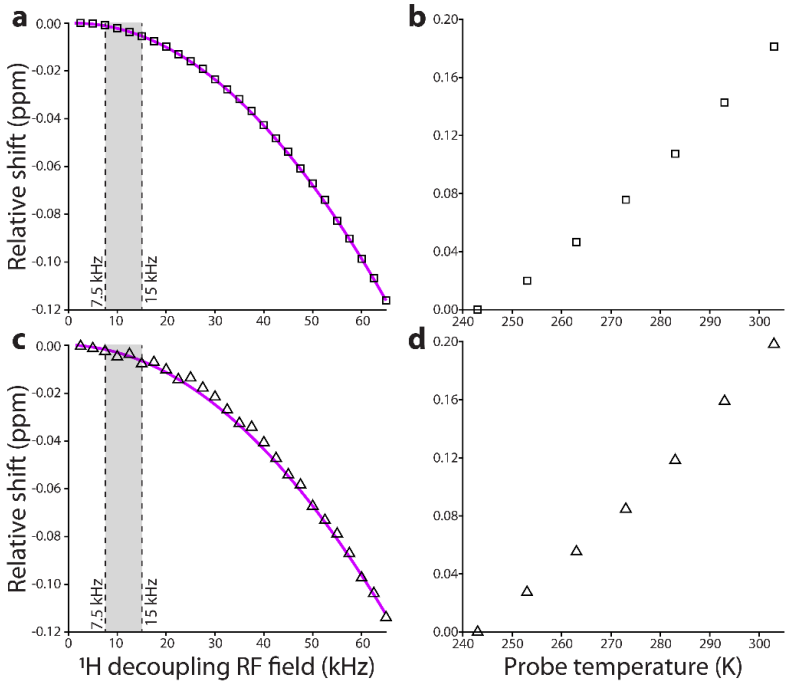

Figure 5. Frequency changes of mefloquine ^{19}F resonances in DP spectra at 100 kHz MAS frequency due to ^{1}H decoupling (a,c) and temperature (b,d). Data for $2CF_3$ and $8CF_3$ ^{19}F peaks are shown by squares (a,b) and triangles (c,d), respectively. The optimal ^{1}H decoupling RF fields (Fig. 4) are shown by the grey area. Magenta lines are the fits of the $2CF_3$ and $8CF_3$ curves data to the equation $y=ax^2+b$. The experimental values of *a* are $-2.75\cdot10^{-11}$ and $-2.66\cdot10^{-11}$ ppm/Hz^2 for the $2CF_3$ and $8CF_3$ resonances, respectively.

2D dipolar-based ^{19}F-detected correlation experiments were also recorded for mefloquine and atorvastatin calcium II as a function of MAS frequency. The ^{19}F-^{19}F fpRFDR and ^{1}H-^{19}F HETCOR spectra of mefloquine acquired at the MAS frequency of 60 and 100 kHz are shown in Fig. 6. As anticipated, spinning at 100 kHz drastically improves the spectral resolution and the sensitivity in both experiments. Quantitative line width and sensitivity enhancement analysis of the 2D ^{19}F-^{19}F fpRFDR spectra is shown in Supporting Information Fig. S1. These enhancements are due to the considerably longer coherence lifetimes for both ^{1}H and ^{19}F nuclei, consistent with prior observations for ^{1}H-based MAS NMR experiments performed at MAS frequencies above 100 kHz [48-51]. We also note that, for the HETCOR experiment, we incorporated a short spin-echo block prior to the ^{1}H chemical shift evolution period (Fig. 2a), to suppress broad signals. As shown in Supporting Information Fig. S2, this T_2 filter cleans up the ^{1}H 1D spectrum and enhances the resolution. Interestingly, the 2D T_2-filtered ^{1}H-^{19}F HETCOR experiment gave rise to both intra- and intermolecular correlations for a CP contact as short as 200 μs, see Supporting Information Fig. S3. These contacts show that the resolution of both ^{1}H and ^{19}F is sufficient to detect crystallographically inequivalent ^{1}H chemical shifts as well. This data set alone is insufficient to

accurately assign all the crystallographically inequivalent ^{1}H-^{19}F cross peaks, but, according to the crystal structure, we estimate that the observed correlations correspond to distances of up to about 5-6 Å.

In comparison with 2D ^{19}F-^{19}F and ^{1}H-^{19}F correlation experiments, their ^{13}C-^{19}F counterparts are considerably more demanding, especially when ^{13}C sites are at natural abundance. ^{13}C-^{19}F spectra are required for chemical shift assignment and structural characterization of fluorinated organic and biological molecules, and thus considerable efforts have been focused on making these experiments accessible [52, 53]. Indeed, we recently demonstrated 2D dipolar-based ^{13}C-^{19}F spectra at frequencies of 60-100 kHz, which rely on ^{13}C-^{19}F CP transfers [19, 20]. While in some systems these are efficient, there are specific examples, notably involving CF_3 groups, where ^{13}C-^{19}F CP is inefficient or fails altogether. Therefore, scalar-based transfers would be highly desirable and in principle should be attainable, given that one-bond ^{19}F-^{13}C scalar couplings, $^{1}J_{FC}$, in many organic molecules are strong, ca. 250 Hz. Gratifyingly, at the MAS frequency of 100 kHz, the coherence lifetimes of ^{13}C and ^{19}F become sufficiently long under ^{1}H decoupling for scalar-based transfers.

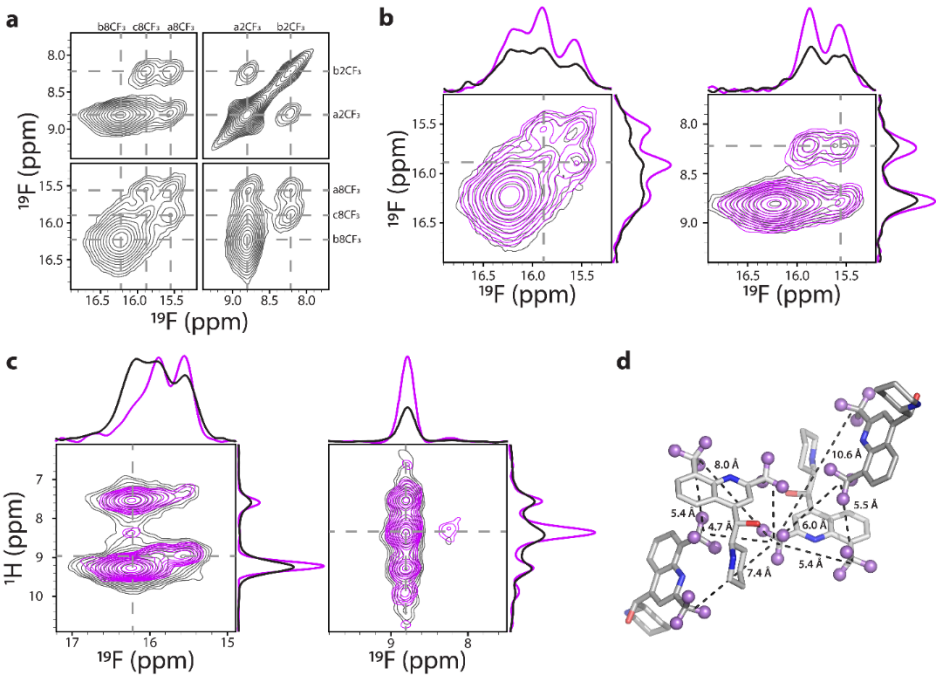

Figure 6. a) 2D ^{19}F-^{19}F fpRFDR spectrum of mefloquine acquired at 100 kHz MAS. The RFDR mixing time was 16 ms. **b)** Expansions of 2D ^{19}F-^{19}F fpRFDR spectra acquired at the MAS frequencies of 60 and 100 kHz, colored grey and magenta, respectively. **c)** Expansions of 2D T_2-filtered ^{1}H-^{19}F HETCOR spectra acquired at the MAS frequencies of 60 and 100 kHz, colored grey and magenta, respectively. In panels (b,c), 1D traces through the 2D spectra are shown at the frequencies shown with grey dash lines. **d)** ^{19}F-^{19}F network in mefloquine crystal with the corresponding intermolecular interfluorine distances depicted in the molecules comprising the unit cell.

Indeed, at the MAS frequency of 100 kHz we have successfully acquired 2D ^{13}C-^{19}F HSQC and HMQC correlation spectra of mefloquine, see Fig. 7. As shown in Fig. 7b, both types of spectra exhibit high resolution, allowing for straightforward assignment of the two CF_3 groups in the molecule and the respective carbon chemical shifts. Naturally, the HSQC and HMQC spectra

provide information on the carbons covalently bonded to fluorines, in contrast to the dipolar-based ^{13}C-detected ^{19}F-^{13}C HETCOR data sets (Fig. 7c). As shown in Fig. 7c, ^{13}C-^{19}F correlations of mefloquine 2CF_3 and 8CF_3 groups are observed in both, the HSQC and HETCOR spectra. The resolution and sensitivity of the ^{19}F-detected HSQC spectrum are high enough to assign the ^{13}C resonances of the crystallographically inequivalent trifluoromethyl groups. Furthermore, the HETCOR spectrum provides through-space ^{13}C-^{19}F correlations unattainable from scalar-based experiments. Taken together, these results illustrate that, ideally, both scalar- and dipolar-based ^{13}C-^{19}F correlation experiments should be acquired, as they provide complementary information for resonance assignments and 3D structure determination.

Finally, both, HSQC and HMQC experiments provide sufficient sensitivity (see Supporting Information Fig. S4), although recoupled multiple quantum coherence in the indirect ^{13}C dimension in the 2D HMQC spectrum results in broader lines (see Supporting Information Figure S5), possibly due to different relaxation in the single- and multiple-quantum coherences [54]. However, the HMQC experiment is more sensitive and thus may be preferred for challenging samples. We note that the relative intensty of mefloquine 2CF_3 peak in the HSQC and HMQC experiments is higher compared to the HETCOR experiment, likely due to its narrower line width (see Fig. 3). While mefloquine 8CF_3 peak has somewhat lower relative intensity in the HSQC and HMQC experiments, it is likely that faster MAS frequencies will give rise to narrower ^{19}F lines and thus higher sensitivity gains in ^{19}F-edited J-based experiments.

2D ^{1}H-^{13}C or ^{13}C-^{1}H HETCOR experiments are often used for structural analysis of organic solids, but the correlations observed in the spectra generally arise from nuclear pairs separated at shorter distances than in the respective 2D ^{1}H-^{19}F and ^{19}F-^{19}F correlation experiments. Generally, ^{19}F-based experiments are significantly more sensitive and can provide correlations corresponding to longer distances of about 2 nm [55], due to the higher gyromagnetic ratios and scarcity of ^{19}F. Moreover, the number of fluorinated moieties is usually considerably smaller than the number of protons in fluorinated organic molecules, thus the ^{19}F-^{13}C correlation experiments demonstrated here exhibit higher resolution and may aid in structural analysis and assignment of ^{13}C resonances.

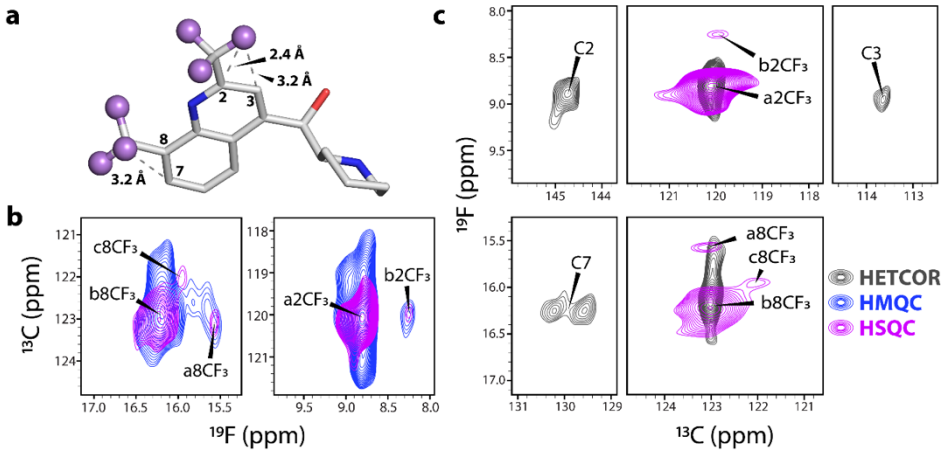

Figure 7. a) Structure of the mefloquine molecule depicting ^{19}F-^{13}C distances of up to 3.2 Å in the X-ray structure. **b)** Scalar-based 2D ^{13}C-^{19}F HSQC (magenta) and HMQC (blue) spectra. **c)** Dipolar-based 2D

^{19}F-^{13}C HETCOR (grey) and scalar-based 2D ^{13}C-^{19}F HSQC (magenta) spectra. All spectra were recorded at 100 kHz MAS. Resonance assignments are indicated.

Naturally, experiments on mefloquine are less challenging than on atorvastatin calcium formulations, given that mefloquine is a pure crystalline compound containing two CF_3 groups, while atorvastatin calcium comes as a 6-9% w/w API in the formulations and has one CF group per molecule. As we have reported recently, atorvastatin calcium I (Teva) and atorvastatin calcium II (Apotex) formulations are both crystalline and comprise different polymorphs [19], each associated with a distinct set of isotropic chemical shifts. The spectrum of atorvastatin calcium II exhibits at least four distinct ^{19}F species with chemical shifts of -36.9, -37.3, -43.5, and -44.1 ppm, representing different crystalline environments, as shown in the ^{19}F MAS spectrum acquired at the MAS frequency of 111 kHz, Fig. 8a. The two peaks centered around -37 and -44 ppm are about 620 Hz wide, considerably broader than in atorvastatin calcium I formulation (Fig. 3b,d). The presence of multiple species is further supported by its 2D ^{19}F-^{19}F fpRFDR spectrum, shown in Fig. 8b. Each of the two broad diagonal peaks consists of multiple resonances. Interestingly, the spectrum exhibits well-resolved cross peaks connecting a subset of peaks, -36.2 to -37.7 and -42.7 to -44.5 ppm. These cross peaks represent correlations within pairs of fluorine atoms with interfluorine distances of 15 Å or shorter [19]. We also note that, due to the long ^{19}F T_1 (23-27 s) in this sample, the DP fpRFDR spectrum shown in Fig. 8b was recorded by accumulating 128 transients per t_1 increment to reach a SNR of 11 in the first FID. Since the ^{1}H T_1 times are considerably shorter, ca. 3.5 s, the incorporation of ^{1}H-^{19}F CP transfer prior to the RFDR mixing period will enable 2D fpRFDR spectra to be recorded in a fraction of time compared to their DP counterparts. For example, in the case of atorvastatin calcium I, the SNR of ^{1}H-^{19}F CP spectrum was about three times higher compared to the DP counterpart, see Fig. 3 caption. Nevertheless, given the low, 9% w/w, API content in atorvastatin calcium II formulation and a total of no more than 40 nanomoles of API in the sample packed in a 0.7 mm rotor, the sensitivity of the fpRFDR experiment is remarkably high.

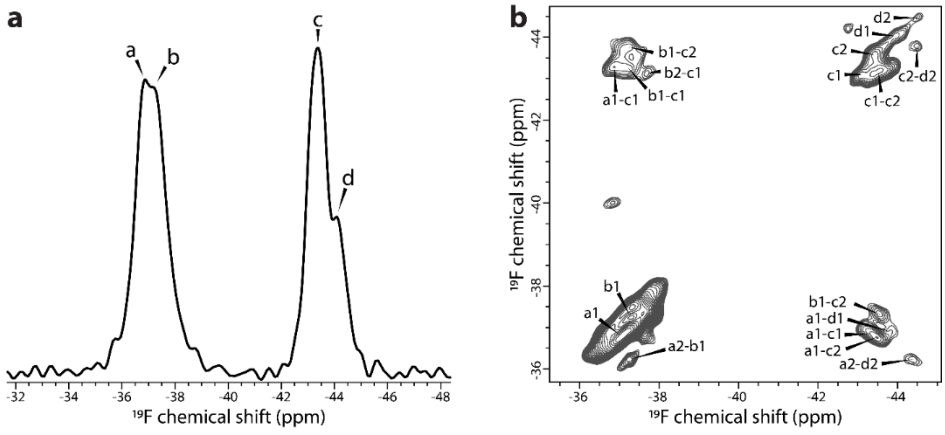

Figure 8. a) 1D ^{19}F DP spectrum of atorvastatin calcium II acquired at the MAS frequency of 111 kHz without ^{1}H decoupling. The spectrum was recorded with 576 scans; the SNR was 40. **b)** 2D ^{19}F-^{19}F fpRFDR spectrum of atorvastatin calcium II acquired at the MAS frequency of 111 kHz without ^{1}H decoupling. The RFDR mixing time was 100 ms.

4. Conclusions

High MAS frequencies of 60-111 kHz are advantageous for ^{19}F solid-state NMR spectroscopy. ^{1}H decoupling during ^{19}F evolution and detection periods results in significant line narrowing, and sufficiently long coherence lifetimes permit scalar-based ^{19}F-^{13}C correlation spectroscopy. ^{1}H-^{19}F dipolar couplings are not fully averaged, even at 111 kHz MAS, necessitating ^{1}H decoupling. Both dipolar- and scalar-based correlation experiments become efficient at 100 kHz MAS, yielding high resolution and sensitivity in a reasonable amount of measurement time. We anticipate that both dipolar- and scalar-based spectra will become important in studies of fluorinated solids and that MAS frequencies faster than 111 kHz will result in additional resolution and sensitivity gains for challenging systems.

Acknowledgments

This work was supported by the National Science Foundation (NSF Grant CHE-1708773) and by the National Institutes of Health (NIH Grant P50AI150481, Technology Development Project 2). We acknowledge that support of the National Institutes of Health (NIH Grant P30GM110758) for the support of core instrumentation infrastructure at the University of Delaware.

Author contributions

T.P. and A.M.G. conceived the project and directed the work. T.P., J.S., G.P.-D., and C.M.Q. designed the MAS NMR experiments. J.S. recorded the MAS NMR data. G.P.-D. analyzed the NMR data. G.P.-D. and T.P. took the lead in writing the manuscript. All authors contributed to the manuscript preparation.

References

[1] Y.G. Gakh, A.A. Gakh, A.M. Gronenborn, Fluorine as an NMR Probe for Structural Studies of Chemical and Biological Systems, Magn. Reson. Chem., 38 (2000) 551-558.

[2] H. Chen, S. Viel, F. Ziarelli, L. Peng, ^{19}F NMR: A Valuable Tool for Studying Biological Events, Chem. Soc. Rev., 42 (2013) 7971-7982.

[3] A.M. Gronenborn, Small, but Powerful and Attractive: ^{19}F in Biomolecular NMR, Structure, 30 (2021) 6-14.

[4] P.B. Crowley, C. Kyne, W.B. Monteith, Simple and Inexpensive Incorporation of ^{19}F-Tryptophan for Protein NMR Spectroscopy, Chem. Commun., 48 (2012) 10681-10683.

[5] N.G. Sharaf, A.M. Gronenborn, Chapter Four - ^{19}F-Modified Proteins and ^{19}F-Containing Ligands as Tools in Solution NMR Studies of Protein Interactions, in: Z. Kelman (Ed.) Methods in Enzymology, Academic Press, 2015, pp. 67-95.

[6] B. Puffer, C. Kreutz, U. Rieder, M.-O. Ebert, R. Konrat, R. Micura, 5-Fluoro Pyrimidines: Labels to Probe DNA and RNA Secondary Structures by 1D ^{19}F NMR Spectroscopy, Nucleic Acids Res., 37 (2009) 7728-7740.

[7] K. Fauster, C. Kreutz, R. Micura, 2′-SCF_3 Uridine—A Powerful Label for Probing Structure and Function of RNA by ^{19}F NMR Spectroscopy, Angew. Chem. Int. Ed., 51 (2012) 13080-13084.

[8] Y. Zhou, J. Wang, Z. Gu, S. Wang, W. Zhu, J.L. Aceña, V.A. Soloshonok, K. Izawa, H. Liu, Next Generation of Fluorine-Containing Pharmaceuticals, Compounds Currently in Phase II–III Clinical Trials of Major Pharmaceutical Companies: New Structural Trends and Therapeutic Areas, Chem. Rev., 116 (2016) 422-518.

[9] H. Mei, J. Han, S. Fustero, M. Medio-Simon, D.M. Sedgwick, C. Santi, R. Ruzziconi, V.A. Soloshonok, Fluorine-Containing Drugs Approved by the FDA in 2018, Chem. Eur. J., 25 (2019) 11797-11819.

[10] M. Inoue, Y. Sumii, N. Shibata, Contribution of Organofluorine Compounds to Pharmaceuticals, ACS Omega, 5 (2020) 10633-10640.

[11] M. Lane Gilchrist, K. Monde, Y. Tomita, T. Iwashita, K. Nakanishi, A.E. McDermott, Measurement of Interfluorine Distances in Solids, J. Magn. Reson., 152 (2001) 1-6.

[12] Y. Koseki, K. Aimi, S. Ando, Crystalline Structure and Molecular Mobility of PVDF Chains in PVDF/PMMA Blend Films Analyzed by Solid-State ^{19}F MAS NMR Spectroscopy, Polym. J., 44 (2012) 757-763.

[13] Q. Chen, K. Schmidt-Rohr, Backbone Dynamics of the Nafion Ionomer Studied by ^{19}F-^{13}C Solid-State NMR, Macromol. Chem. Phys., 208 (2007) 2189-2203.

[14] B. Kwon, M. Roos, V.S. Mandala, A.A. Shcherbakov, M. Hong, Elucidating Relayed Proton Transfer through a His–Trp–His Triad of a Transmembrane Proton Channel by Solid-State NMR, J. Mol. Biol., 431 (2019) 2554-2566.

[15] X. Lu, D. Skomski, K.C. Thompson, M.J. McNevin, W. Xu, Y. Su, Three-Dimensional NMR Spectroscopy of Fluorinated Pharmaceutical Solids under Ultrafast Magic Angle Spinning, Anal. Chem., 91 (2019) 6217-6224.

[16] V.S. Mandala, M.J. McKay, A.A. Shcherbakov, A.J. Dregni, A. Kolocouris, M. Hong, Structure and Drug Binding of the SARS-CoV-2 Envelope Protein Transmembrane Domain in Lipid Bilayers, Nat. Struct. Mol. Biol., 27 (2020) 1202-1208.

[17] A.A. Shcherbakov, G. Hisao, V.S. Mandala, N.E. Thomas, M. Soltani, E.A. Salter, J.H. Davis, K.A. Henzler-Wildman, M. Hong, Structure and Dynamics of the Drug-Bound Bacterial Transporter EmrE in Lipid Bilayers, Nat. Commun., 12 (2021) 172.

[18] M. Lu, S. Sarkar, M. Wang, J. Kraus, M. Fritz, C.M. Quinn, S. Bai, S.T. Holmes, C. Dybowski, G.P.A. Yap, J. Struppe, I.V. Sergeyev, W. Maas, A.M. Gronenborn, T. Polenova, ^{19}F Magic Angle Spinning NMR Spectroscopy and Density Functional Theory Calculations of Fluorosubstituted Tryptophans: Integrating Experiment and Theory for Accurate Determination of Chemical Shift Tensors, J. Phys. Chem. B, 122 (2018) 6148-6155.

[19] C.M. Quinn, R. Zadorozhnyi, J. Struppe, I.V. Sergeyev, A.M. Gronenborn, T. Polenova, Fast ^{19}F Magic-Angle Spinning Nuclear Magnetic Resonance for the Structural Characterization of Active Pharmaceutical Ingredients in Blockbuster Drugs, Anal. Chem., 93 (2021) 13029-13037.

[20] C. Guo, M.P. Fritz, J. Struppe, S. Wegner, J. Stringer, I.V. Sergeyev, C.M. Quinn, A.M. Gronenborn, T. Polenova, Fast ^{19}F Magic Angle Spinning NMR Crystallography for Structural Characterization of Fluorine-Containing Pharmaceutical Compounds, Anal. Chem., 93 (2021) 8210-8218.

[21] M. Fritz, J. Kraus, C.M. Quinn, G.P.A. Yap, J. Struppe, I.V. Sergeyev, A.M. Gronenborn, T. Polenova, Measurement of Accurate Interfluorine Distances in Crystalline Organic Solids: A High-Frequency Magic Angle Spinning NMR Approach, J. Phys. Chem. B, 123 (2019) 10680-10690.

[22] M. Lu, M. Wang, I.V. Sergeyev, C.M. Quinn, J. Struppe, M. Rosay, W. Maas, A.M. Gronenborn, T. Polenova, ^{19}F Dynamic Nuclear Polarization at Fast Magic Angle Spinning for NMR of HIV-1 Capsid Protein Assemblies, J. Am. Chem. Soc., 141 (2019) 5681-5691.

[23] M. Wang, M. Lu, M.P. Fritz, C.M. Quinn, I.-J.L. Byeon, C.-H. Byeon, J. Struppe, W. Maas, A.M. Gronenborn, T. Polenova, Fast Magic-Angle Spinning ^{19}F NMR Spectroscopy of HIV-1 Capsid Protein Assemblies, Angew. Chem. Int. Ed., 57 (2018) 16375-16379.

[24] Y. Du, Y. Su, ^{19}F Solid-State NMR Characterization of Pharmaceutical Solids, Solid State Nucl. Magn. Reson., 120 (2022) 101796.

[25] E. Matei, A.M. Gronenborn, ^{19}F Paramagnetic Relaxation Enhancement: A Valuable Tool for Distance Measurements in Proteins, Angew. Chem. Int. Ed., 55 (2016) 150-154.

[26] G.B. Crull, J.W. Kennington, A.R. Garber, P.D. Ellis, J.H. Dawson, ^{19}F Nuclear Magnetic Resonance as a Probe of the Spatial Relationship between the Heme Iron of Cytochrome P-450 and Its Substrate, J. Biol. Chem., 264 (1989) 2649-2655.

[27] M.C. Loewen, J. Klein-Seetharaman, E.V. Getmanova, P.J. Reeves, H. Schwalbe, H.G. Khorana, Solution ^{19}F Nuclear Overhauser Effects in Structural Studies of the Cytoplasmic Domain of Mammalian Rhodopsin, Proc. Natl. Acad. Sci. U.S.A., 98 (2001) 4888-4892.

[28] L. Liang, Y. Ji, K. Chen, P. Gao, Z. Zhao, G. Hou, Solid-State NMR Dipolar and Chemical Shift Anisotropy Recoupling Techniques for Structural and Dynamical Studies in Biological Systems, Chem. Rev., 122 (2022) 9880-9942.

[29] H. Saitô, I. Ando, A. Ramamoorthy, Chemical Shift Tensor – the Heart of NMR: Insights into Biological Aspects of Proteins, Prog. Nucl. Magn. Reson. Spectrosc., 57 (2010) 181-228.

[30] P. Schanda, M. Ernst, Studying Dynamics by Magic-Angle Spinning Solid-State NMR Spectroscopy: Principles and Applications to Biomolecules, Prog. Nucl. Magn. Reson. Spectrosc., 96 (2016) 1-46.

[31] G. Porat-Dahlerbruch, J. Struppe, C.M. Quinn, A.M. Gronenborn, T. Polenova, Determination of Accurate ^{19}F Chemical Shift Tensors with R-Symmetry Recoupling at High MAS Frequencies (60–100 kHz), J. Magn. Reson., 340 (2022) 107227.

[32] A.A. Shcherbakov, V.S. Mandala, M. Hong, High-Sensitivity Detection of Nanometer ^{1}H–^{19}F Distances for Protein Structure Determination by ^{1}H-Detected Fast MAS NMR, J. Phys. Chem. B, 123 (2019) 4387-4391.

[33] M. Roos, V.S. Mandala, M. Hong, Determination of Long-Range Distances by Fast Magic-Angle-Spinning Radiofrequency-Driven ^{19}F–^{19}F Dipolar Recoupling NMR, J. Phys. Chem. B, 122 (2018) 9302-9313.

[34] A.E. Bennett, R.G. Griffin, J.H. Ok, S. Vega, Chemical Shift Correlation Spectroscopy in Rotating Solids: Radio Frequency-Driven Dipolar Recoupling and Longitudinal Exchange, J. Chem. Phys., 96 (1992) 8624-8627.

[35] A.E. Bennett, C.M. Rienstra, J.M. Griffiths, W. Zhen, P.T.L. Jr., R.G. Griffin, Homonuclear Radio Frequency-Driven Recoupling in Rotating Solids, J. Chem. Phys., 108 (1998) 9463-9479.

[36] Y. Ishii, ^{13}C–^{13}C Dipolar Recoupling under Very Fast Magic Angle Spinning in Solid-State Nuclear Magnetic Resonance: Applications to Distance Measurements, Spectral Assignments, and High-Throughput Secondary-Structure Determination, J. Chem. Phys., 114 (2001) 8473-8483.

[37] M. Shen, B. Hu, O. Lafon, J. Trébosc, Q. Chen, J.-P. Amoureux, Broadband Finite-Pulse Radio-Frequency-Driven Recoupling (fp-RFDR) with (XY8)4^{1} Super-Cycling for Homo-Nuclear Correlations in Very High Magnetic Fields at Fast and Ultra-Fast MAS Frequencies, J. Magn. Reson., 223 (2012) 107-119.

[38] D. Marion, M. Ikura, R. Tschudin, A. Bax, Rapid Recording of 2D NMR Spectra without Phase Cycling. Application to the Study of Hydrogen Exchange in Proteins, J. Magn. Reson., 85 (1989) 393-399.

[39] A.E. Bennett, C.M. Rienstra, M. Auger, K.V. Lakshmi, R.G. Griffin, Heteronuclear Decoupling in Rotating Solids, J. Chem. Phys., 103 (1995) 6951-6958.

[40] B.M. Fung, A.K. Khitrin, K. Ermolaev, An Improved Broadband Decoupling Sequence for Liquid Crystals and Solids, J. Magn. Reson., 142 (2000) 97-101.

[41] M. Kotecha, N.P. Wickramasinghe, Y. Ishii, Efficient Low-Power Heteronuclear Decoupling in ^{13}C High-Resolution Solid-State NMR under Fast Magic Angle Spinning, Magn. Reson. Chem., 45 (2007) S221-S230.

[42] M. Mehring, Principles of High Resolution NMR in Solids, Springer Verlag, Berlin, 1983.

[43] S.A. Vierkötter, Applications of the Bloch–Siegert Shift in Solid-State Proton-Dipolar-Decoupled ^{19}F MAS NMR, J. Magn. Reson., 118 (1996) 84-93.

[44] MATLAB and Curve Fitting Toolbox Release 2021a, Mathworks, Inc., Natick, Massachusetts, United States,

[45] F. Bloch, A. Siegert, Magnetic Resonance for Nonrotating Fields, Phys. Rev., 57 (1940) 522-527.

[46] N.F. Ramsey, Resonance Transitions Induced by Perturbations at Two or More Different Frequencies, Phys. Rev., 100 (1955) 1191-1194.

[47] S.H. Autler, C.H. Townes, Stark Effect in Rapidly Varying Fields, Phys. Rev., 100 (1955) 703-722.

[48] J. Struppe, C.M. Quinn, M. Lu, M. Wang, G. Hou, X. Lu, J. Kraus, L.B. Andreas, J. Stanek, D. Lalli, A. Lesage, G. Pintacuda, W. Maas, A.M. Gronenborn, T. Polenova, Expanding the Horizons for Structural Analysis of Fully Protonated Protein Assemblies by NMR Spectroscopy at MAS Frequencies above 100 khz, Solid State Nucl. Magn. Reson., 87 (2017) 117-125.

[49] D. Cala-De Paepe, J. Stanek, K. Jaudzems, K. Tars, L.B. Andreas, G. Pintacuda, Is Protein Deuteration Beneficial for Proton Detected Solid-State NMR at and above 100 kHz Magic-Angle Spinning?, Solid State Nucl. Magn. Reson., 87 (2017) 126-136.

[50] S. Penzel, A.A. Smith, V. Agarwal, A. Hunkeler, M.-L. Org, A. Samoson, A. Böckmann, M. Ernst, B.H. Meier, Protein Resonance Assignment at MAS Frequencies Approaching 100 kHz: A Quantitative Comparison of J-Coupling and Dipolar-Coupling-Based Transfer Methods, J. Biomol. NMR, 63 (2015) 165-186.

[51] M. Schledorn, A.A. Malär, A. Torosyan, S. Penzel, D. Klose, A. Oss, M.-L. Org, S. Wang, L. Lecoq, R. Cadalbert, A. Samoson, A. Böckmann, B.H. Meier, Protein NMR Spectroscopy at 150 kHz Magic-Angle Spinning Continues to Improve Resolution and Mass Sensitivity, ChemBioChem, 21 (2020) 2540-2548.

[52] A.A. Shcherbakov, M. Hong, Rapid Measurement of Long-Range Distances in Proteins by Multidimensional ^{13}C–^{19}F REDOR NMR under Fast Magic-Angle Spinning, J. Biomol. NMR, 71 (2018) 31-43.

[53] A.A. Shcherbakov, M. Roos, B. Kwon, M. Hong, Two-Dimensional ^{19}F–^{13}C Correlation NMR for ^{19}F Resonance Assignment of Fluorinated Proteins, J. Biomol. NMR, 74 (2020) 193-204.

[54] A. Bax, M. Ikura, L.E. Kay, D.A. Torchia, R. Tschudin, Comparison of Different Modes of Two-Dimensional Reverse-Correlation NMR for the Study of Proteins, J. Magn. Reson., 86 (1990) 304-318.

[55] A.A. Shcherbakov, J. Medeiros-Silva, N. Tran, M.D. Gelenter, M. Hong, From Angstroms to Nanometers: Measuring Interatomic Distances by Solid-State NMR, Chem. Rev., 122 (2022) 9848-9879.